Genome Medicine

RESEARCH

Open Access

Epigenomic preconditioning of peripheral monocytes determines their transcriptional response to the tumor microenvironment

Máté Kiss[1,2,3,13*†], Laszlo Halasz[4,14†], Eva Hadadi[1,2,3†], Wilhelm K. Berger[4], Petros Tzerpos[5], Szilard Poliska[5], Daliya Kancheva[1,2,3], Aurélie Gabriel[6], Romina Mora Barthelmess[1,2], Ayla Debraekeleer[2,3], Jan Brughmans[2,3], Yvon Elkrim[1,2], Liesbet Martens[7,8], Yvan Saeys[7,9], Bence Daniel[10], Zsolt Czimmerer[11,12], Damya Laoui[2,3†], Laszlo Nagy[4,5†] and Jo A. Van Ginderachter[1,2*†]

Abstract

Background Monocytes are recruited to tumors and undergo transcriptional reprogramming resulting in tumor-promoting functions. Epigenomic features, such as post-translational modification of histones and chromatin accessibility, are key determinants of transcription factor binding and thereby play an important role in controlling transcriptional responses to the tissue environment. It remains unknown whether systemic tumor-associated signals could alter the epigenomic landscape of peripheral monocytes before they reach the tumor, thus shaping their subsequent response to the tumor microenvironment.

Methods We used a combination of genome-wide assays for chromatin accessibility and multiple histone modifications (H3K4me1, H3K4me3, H3K27ac) in a mouse tumor model to investigate changes in the epigenomic landscape of peripheral monocytes. We then integrated these epigenomic data with transcriptomic data to link altered regulatory elements to gene expression changes in monocytes occurring in the periphery or during tumor infiltration.

Results We found that tumor-induced systemic inflammation was associated with transcriptional and epigenomic preconditioning of peripheral monocytes. The distal tumor caused extensive remodeling of both H3K4me3$^+$ promoters and H3K4me1$^+$ enhancers. Specifically, this involved the repression of interferon-responsive regulatory elements as well as the establishment of enhancers harboring binding motifs for transcription factor families downstream of pro-inflammatory signaling, such as C/EBP, AP-1, and STAT. Reprogrammed enhancers in peripheral monocytes were linked to sustained gene expression changes that persisted after tumor infiltration. In addition, key pro-tumor genes upregulated in tumor-infiltrating monocytes showed epigenetic priming already in the circulation.

†Máté Kiss, Laszlo Halasz and Eva Hadadi contributed equally to this work.

†Damya Laoui, Laszlo Nagy and Jo A. Van Ginderachter are senior authors.

*Correspondence:
Máté Kiss
mate.kiss@unige.ch
Jo A. Van Ginderachter
jo.van.ginderachter@vub.be
Full list of author information is available at the end of the article

Conclusions These results suggest that cancer-associated remodeling of the epigenomic landscape in peripheral monocytes can shape the gene expression programs they acquire in the tumor, highlighting the role of the epigenome in redirecting monocyte function to support cancer progression.

Keywords Cancer, Monocyte, Epigenome, Transcriptome, Enhancer, Histone

Background

Classical monocytes play an essential role in host defense through their ability to rapidly migrate to sites of injury or infection where they initiate an inflammatory response [1]. Similar to inflamed tissues, classical monocytes are mobilized to tumors where they either differentiate into tumor-associated macrophages or accumulate without differentiation, depending on the cytokine milieu [2, 3]. Both monocytes and monocyte-derived macrophages can exert tumor-promoting activities, including suppression of anti-tumor T-cell responses, promotion of angiogenesis, and facilitation of metastatic colonization [3]. These activities arise due to extensive transcriptional reprogramming of monocytes when transitioning from the blood to the tumor, involving the activation of genes encoding inflammatory cytokines, pro-angiogenic factors, and growth factors [4–7]. However, recruited monocytes can also acquire an immunostimulatory phenotype and promote anti-tumor immunity in certain contexts. Specifically, the presence of type I interferon in the tumor can induce an immunostimulatory phenotype which supports the anti-tumor T-cell response [8, 9]. Such interferon-responsive monocytes can also be detected during the course of successful cancer immunotherapies, and their abundance is associated with a better response to treatment [9–12]. Overall, these observations indicate that the transcriptional response of monocytes to microenvironmental signals is paramount in determining their phenotype and consequently their impact on disease outcome.

It is increasingly appreciated that cancer can disrupt immune homeostasis not only locally but also systemically [13]. Indeed, multiple studies have demonstrated that modulation of monocyte function in cancer occurs already prior to their infiltration into the tumor [14]. Phenotypic changes that have been observed in multiple tumor types include the acquisition of immunosuppressive activity and reduced responsiveness to interferon stimulation [14–18]. Peripheral blood monocytes from cancer patients show a distinct gene expression profile compared to healthy controls, and these changes are largely cancer type-specific [19, 20]. Importantly, transcriptional alterations in blood monocytes can also be detected in patients with localized early-stage tumors [20].

Although transcriptomic changes in peripheral monocytes in the context of cancer are well documented, it is currently unknown to what extent the epigenomic landscape of monocytes is altered by a distant tumor. Epigenomic features, such as post-translational modification of histones and chromatin accessibility, are key determinants of DNA binding and thus genome-wide localization and activity of transcription factors activated by external signals [21]. The preformed epigenomic landscape determined by these features plays a key role in directing transcriptional responses to the cues of the microenvironment. Importantly, epigenetic marks are typically less dynamic than the activity of upstream signaling pathways and can therefore convert transient signals into long-lasting transcriptional alterations or transcriptional memory by acting as bookmarks which could persist even after cessation of the stimulus [22, 23]. The preformed epigenomic landscape is likely to be important in shaping the responses of monocytes when they encounter new signals upon tumor infiltration. Nonetheless, it remains unknown whether some tumor-induced transcriptional changes already in peripheral monocytes could be programmed at the epigenomic level and whether epigenomic changes could prime genes for activation upon tumor infiltration.

In this study, we aimed to address these knowledge gaps in a murine model by using an array of complementary genome-wide assays for mRNA expression (RNA-seq), histone modifications (H3K4me3 CUT&Run, H3K4me1, and H3K27ac CUT&Tag) and chromatin accessibility (ATAC-seq) to detect potential cancer-induced changes in the epigenomic landscape of peripheral monocytes and link these to gene expression changes occurring in the periphery or upon tumor infiltration.

Methods

Mice

All experiments were performed with age-matched female mice. C57BL/6 J mice were from Janvier. All procedures followed the guidelines of the Belgian Council for Laboratory Animal Science and were approved by the Ethical Committee for Animal Experiments of the Vrije Universiteit Brussel (licenses 15–220-3 and 19–220-8). Mice were kept in conventional cages, on a 12-h light/dark cycle, with water and food ad libitum. Euthanasia was performed using carbon dioxide inhalation.

Tumor models and animal cohorts

For tumor implantation, 3×10^6 Lewis lung carcinoma (LLC) were injected subcutaneously into the right flank of mice in HBSS. Blood and tumors were collected 16–17 days after tumor implantation. Immune profiling was performed, and $CD11b^+Ly6G^-Ly6C^{hi}MHC\text{-}II^-$ monocytes were sorted for downstream analyses from the blood and tumor of tumor-bearing mice as well as the blood of age-matched healthy mice. Separate mouse cohorts were used for each downstream assay. Plasma was collected from multiple mouse cohorts for cytokine measurements. The sorted cell numbers and the number of replicates in each cohort are indicated below in the description of the downstream assays.

Cell lines

LLC cells were from ATCC. LLC-eGFP cells were generated previously [24]. The cell lines were maintained in DMEM (Gibco) supplemented with 10% (v/v) heat-inactivated fetal calf serum (FCS; Capricorn Scientific), 300 µg/ml L-glutamine (Sigma), 100 units/ml penicillin, and 100 µg/ml streptomycin (Gibco).

Blood collection and tumor dissociation

Blood was collected from mice in 1 ml syringes containing 0.5 mol/L EDTA. Plasma was separated by centrifugation and collected for cytokine measurements. For immune profiling, 3 µl blood was collected through a tail snip. Red blood cells were lysed using Ammonium–Chloride–Potassium (ACK) lysis buffer. Tumors were excised, cut into small pieces, incubated with 10 U/ml collagenase I (Worthington), 400 U/ml collagenase IV (Worthington) and 30 U/ml DNase I (Worthington) in RPMI for 30 min at 37 °C, squashed, and filtered. Following red blood cell lysis with ACK buffer, LymphoPrep density gradient was used to remove debris and dead cells.

Cell sorting

Blood and tumor cell suspensions were resuspended in HBSS with 2 mmol/L EDTA and 0.5% (v/v) FCS. To prevent nonspecific antibody binding to Fcγ receptors, cells were pre-incubated with CD16/CD32-specific antibody (clone 2.4G2). Cell suspensions were then incubated with fluorescently labelled antibodies diluted in HBSS with 2 mmol/L EDTA and 1% (v/v) FCS for 20 min at 4 °C and then washed with the same buffer. The following fluorochrome-conjugated antibody clones were used: CD11b (M1/70), Ly6G (1A8), Ly6C (HK1.4), MHC-II (M5/114.15.2). $Ly6C^{hi}$ monocytes were gated as $CD11b^+Ly6G^-Ly6C^{hi}MHC\text{-}II^-$ cells. All macrophages in LLC tumors are $Ly6C^-$ and were therefore excluded [25]. Fluorescence-activated cell sorting was performed using a BD FACSAria II (BD Biosciences).

Cytokine measurements

The following cytokines were measured by ELISA ($n = 9$–10 mice/group): IL-1β (R&D Systems #MHSSLB00), IL-4 (R&D Systems #DY404), IL-6 (Biolegend #431,317), IL-36α (R&D Systems #DY2297), IL-36β (R&D Systems #DY2298), GM-CSF (R&D Systems #DY415), TNFα (R&D Systems #DY410), IFNγ (R&D Systems #DY485). IL-1α, IL-33, and G-CSF were measured in plasma using multiplex immunoassay (Bio-Rad, #171G5001M, #171G5002, #171G5015M, respectively). All measurements were performed according to the manufacturers' protocol.

Kinetic immune profiling of blood and tumor samples

Peripheral blood was collected from healthy mice at 7, 10, and 16 days after tumor inoculation ($n = 6$–8 mice/group at each time point). Tumors were collected and processed at 7, 10, and 15 days post-inoculation ($n = 4$ mice/time point). Following RBC lysis and viability stain (BD Horizon Fixable Viability Stain 575 V #565,694) the cells were pre-incubated with CD16/CD32-specific antibody (clone 2.4G2). Cell suspensions were then incubated with fluorescently labelled antibodies and analyzed with flow cytometer (BD Symphony A3). Within live $CD45^+$ cells, the following immune cell populations were identified: $Ly6C^{hi}$ monocytes ($CD11b^+Ly6G^-SiglecF^-MHCII^-F4/80^-Ly6C^{hi}$), macrophages ($CD11b^+Ly6G^-SiglecF^-Ly6C^{low}F4/80^+$), neutrophils ($CD11b^+Ly6G^+$), cDC1 ($Ly6G^-CD11c^+MHCII^+SiglecH^-CD88^-CD64^-F4/80^-CD11b^-XCR1^+$), cDC2 ($Ly6G^-CD11c^+MHCII^+SiglecH^-CD88^-CD64^-F4/80^-CD11b^+XCR1^-$), B cells ($CD19^+B220^+$), NK cells ($TCRb^-NK1.1^+$), $CD4^+$ T cells ($CD11b^-TCR\beta^+CD4^+$), $CD8^+$ T cells ($CD11b^-TCR\beta^+CD8^+$). The following antibodies were used: CD45 (clone 30-F11, BD #748,370), Ly6G (clone 1A8, BD #612,921), CD19 (clone 1D3, BD #563,157), B220 (clone RA3-6B2, Biolegend #103,210), CD11b (clone M1/70, Biolegend #101,239), SiglecF (clone E20-2440, BD #740,388), SiglecH (clone 440c, BD #747,668), CD11c (clone HL3, BD #550,261 and clone N418, Biolegen #117,318), MHCII (clone 2G9, BD # 743,876), XCR1 (clone ZET, BD #148,216), CD3e (clone 145-2C11, BD #612,771), TCRβ (clone H57-597, BD #612,821), CD4 (clone RM4-5, Biolegend #100,559), CD8a (clone 53–6.7, BD #750,024), NK1.1 (clone PK136, BD #7,441,477), Ly6C (clone AL-21, BD #560,596), CD88 (clone REA1206, Miltenyi Biotec #130–106-122), CD64 (clone

X54-5/7.1, Biolegend #139,303), F4/80 (clone T45-2342, BD #565,787).

T cell suppression assay

Single-cell suspension of spleens was prepared by squashing the spleens between two 100-µm mesh filters. Following red blood cell lysis, splenocytes were counted and labelled with CellTrace Violet (Invitrogen #C34557). The labelled splenocytes were resuspended in complete medium (RPMI with 10% FCS, 1% P/S, 1% glutamine supplemented with 1% sodium-pyruvate, 1% NEAA, and 0.003% beta-mercaptoethanol). T cell activation was induced by CD3/C28 beads (Dynabeads™ Mouse T-Activator CD3/CD28, Gibco #1146D). CD3/CD28 beads were prepared and used according to the manufacturer's instructions. Splenocytes and sorted monocytes were co-cultured at a 1:1 ratio (100,000 splenocytes: 100,000 sorted monocytes) for 42 h in a 96-well flat bottom plate ($n=6$ T-cell donor animals/condition, data pooled from two independent experiments). For sample collection, the plate was centrifuged at 450 g for 5 min; then, the supernatant was collected and kept for ELISA measurement. The cells were washed off in HBSS with 2 mM EDTA and 0.5% (v/v) FCS and stained for flow cytometry analysis with TCRβ (clone H57-597, Invitrogen #11–5961-85), CD4 (clone RM4-5, Biolegend #100,516), CD8a (clone 53–6.7, BD #553,033) and CD44 (clone IM7, Biolegend #103,029).

Monocyte—cancer cell co-culture

For co-culture with monocytes, 500 LLC-eGFP cells were added in 100 µl culture medium in a 96-well flat-bottom plate the day before the start of the co-culture. The next day, 5000 sorted monocytes were added in 100 µl culture medium ($n=12$ replicates, data pooled from two independent experiments). The plate was placed in a Cytation 10 Confocal image reader (Agilent BioTek) and the wells were imaged in 2 h intervals for 78 h using a 4× objective. Cancer cell growth was assessed based on the detected GFP signal (ratio of GFP area compared to the total imaged area). Image analysis was performed in the Gen5 Image Prime 3.16 software (Agilent Biotek).

RNA-seq

RNA-seq was performed in three biological replicates per group. RNA from sorted cells was isolated using TRIzol reagent (Invitrogen) according to the manufacturer's instructions. RNA-Seq libraries were prepared using the TruSeq RNA Sample Preparation Kit (Illumina) according to the manufacturer's protocol. Libraries were sequenced with the Illumina HiScanSQ sequencer.

RNA-seq data analysis

Raw sequencing reads were processed by the nfcore RNA-seq pipeline (v3.10.1) with default parameters [26]. Briefly, the reads were trimmed with trimgalore (v0.6.7) and cutadapt (v3.4) then mapped to the *mm10* genome using STAR (v2.6.1d) [27] and quantified with Salmon (v1.9.0) [28]. Genes with low counts were removed using edgeR's filterByExpr function (*min.count=3*) [29]. Principal component analysis (PCA) was performed using PCATools R package (*removeVar=0.1*). EdgeR was used for normalization and differential gene expression analysis with a threshold of FDR less than 0.05 and absolute $\log_2$ fold-change greater than 0.5. *K*-means clustering ($k=6$) and heatmaps were generated using pheatmap. We used EnrichR for functional annotation of clusters against the MSigDB Hallmark 2020 database [30]. Monocyte polarization state and cytokine drivers were predicted using the Immune Response Enrichment Analysis (IREA) [31] tool using the list of significantly upregulated genes (FDR < 0.05, log2FC > 0.5). The regulatory activity of transcription factors (TFs) was inferred using the Univariate Linear Model (ULM) approach from decoupleR (R package version 2.12.0) [32]. The'run_ulm'function was run on the log-transformed TPM values and with the CollecTRI network containing a curated collection of TFs and their gene targets as prior knowledge.

ATAC-seq

ATAC-seq was performed in three biological replicates per group. ATAC-seq was carried out as described earlier with minor modifications [33]. Fifty thousand Ly6C^{hi} monocytes were sorted into ice-cold PBS. After centrifugation, the cell pellet was resuspended in ATAC lysis buffer (10 mmol/L Tris–HCl pH7.4, 10 mmol/L NaCl, 3 mmol/L MgCl2, 0.1% IGEPAL). After centrifugation, cell nuclei were tagmented using the Nextera DNA Library Preparation Kit (Illumina). After tagmentation, DNA was purified with the MinElute PCR Purification Kit (QIAGEN). Tagmented DNA was amplified with the Kapa Hifi Hot Start Kit (Kapa Biosystems) using 9 PCR cycles. Amplified libraries were purified again with the MinElute PCR Purification Kit. Fragment distribution of libraries was assessed with the Agilent Bioanalyzer and libraries were sequenced on a HiSeq 2500 platform.

ATAC-seq data analysis

Raw sequencing reads were processed by the nfcore ATAC-seq pipeline (v1.2.1) with default parameters. Briefly, the reads were trimmed with trimgalore (v0.6.4_dev) then mapped to the *mm10* genome using BWA (v0.7.17-r1188). Low quality reads and reads mapping

to blacklisted regions were discarded. Duplicated reads were merged. We used MACS2 [34] to identify significantly enriched genomic regions using FDR 5%.

H3K4me3 CUT&Run

Sorted Ly6C^{hi} monocytes (100,000 cells per condition in two replicates) were cryopreserved in ice cold cryopreservation solution consisting of 50% FBS, 40% complete RPMI and 10% DMSO. The CUT&RUN protocol was performed using the Epicypher CUTANA CUT&RUN kit according to the manufacturer's instructions with some minor modifications. Briefly, monocytes were recovered from freezing media by quickly thawing samples at 37 °C. Cells were spun down at 600 g for 3 min at room temperature. Cells were then resuspended in 105 µl of room temperature wash buffer and cell viability was confirmed. Cells were then incubated with concavilin A beads for 10 min at room temperature. 0.5 µg of antibodies for target proteins were then added and incubated overnight on nutator at 4 °C. The following day, cells were washed with cell permeabilization buffer, before the addition of the pAG-MNase. Cells were incubated with the pAG-MNase for 10 min at room temperature. To digest and release target chromatin, 100 mM Calcium Chloride was added to the reaction. After a 2-h incubation on nutator at 4 °C, the reaction was halted by the addition of a stop mastermix. Reactions were placed on a thermocycler at 37 °C for 10 min. DNA was purified using SPRISelect beads (1.4×volume). Libraries were then prepared with Epicypher's CUT&RUN Library Prep Kit according to the manufacturer's protocol and then subjected to paired-end sequencing on a NextSeq2000 machine (1×50 bp reads).

H3K4me1 and H3K27ac CUT&Tag

Sorted Ly6C^{hi} monocytes (200,000 cells per condition in two replicates) were cryopreserved in ice-cold cryopreservation solution consisting of 50% FBS, 40% complete RPMI, and 10% DMSO. Cryopreserved samples were sent to Active Motif for CUT&Tag in two replicates. Thawed cells were incubated overnight with Concanavalin A beads and 1 µl of the primary anti-H3K4me1 antibody per reaction (Active Motif, catalog number 39297) and 1 µl of the primary anti-H3K27ac antibody per reaction (Active Motif, catalog number 39135). After incubation with the secondary anti-rabbit antibody (1:100), cells were washed, and tagmentation was performed at 37 ℃ using protein-A-Tn5. Tagmentation was halted by the addition of EDTA, SDS, and proteinase K at 55 ℃, after which DNA extraction and ethanol purification were performed, followed by PCR amplification and barcoding (see Active Motif CUT&Tag kit, catalog number 53160 for recommended conditions and indexes). Following SPRI bead cleanup (Beckman Coulter), the resulting DNA libraries were quantified and sequenced on Illumina's NextSeq 550 (PE38).

CUT&Run and CUT&Tag data analysis

Raw sequencing reads were processed by the nfcore cutandrun pipeline (v3.0.0) with default parameters. Briefly, the reads were trimmed with trimgalore (v0.6.6) then mapped to the *mm10* genome using Bowtie2 (v2.4.4). Low quality reads and reads mapping to blacklisted regions were discarded. Duplicated reads were merged. We used MACS2 to identify significantly enriched genomic regions using FDR 5%. Genomic annotation of the peaks was done using ChIPseeker [35]. We used DiffBind (filter = 3, minOverlap = 2) to identify differential genomic regions using edgeR. Distance to nearest DEG's transcription start site (TSS) was calculated using plyranges (± 100 kb). Coverage files were created using deepTools, normalized with RPKM. Read density plots and corresponding boxplot quantification were calculated by deepTools and profileplyr. For motif enrichment analyses, we used HOMER findMotifsGenome.pl with default parameters or monaLisa [36].

Results

Tumor-induced systemic inflammation is associated with transcriptional preconditioning of peripheral monocytes

In order to determine potential links between peripheral alterations in monocytes and their local reprogramming in the tumor, we sought to identify genes whose expression was modulated by the tumor either in the periphery or upon tumor infiltration. To this end, we performed bulk RNA-sequencing on CD11b^{hi} Ly6C^{hi} Ly6G^{-} MHC-II^{-} classical monocytes isolated from the tumor and blood of Lewis lung carcinoma (LLC) tumor-bearing mice as well as from the blood of healthy syngeneic mice (Fig. 1A). The comparison between cells from genetically identical tumor-bearing and healthy mice allowed us to exclude the impact of genetic variation and precisely identify tumor-induced changes in the gene expression of peripheral monocytes (Fig. 1A). The LLC model was chosen as this tumor recruits a large number of monocytes which show immunosuppressive features [25]. Indeed, we observed that progressive LLC tumors increased systemic Ly6C^{hi} monocyte levels and gradually accumulated large numbers of macrophages (Additional file 1: Fig. S1A, B).

We found that the transcriptome of tumor-infiltrating monocytes was very different from monocytes in the blood, while the tumor also induced distinct, albeit less pronounced, changes in the transcriptome of peripheral monocytes (Fig. 1A, B). A fraction of

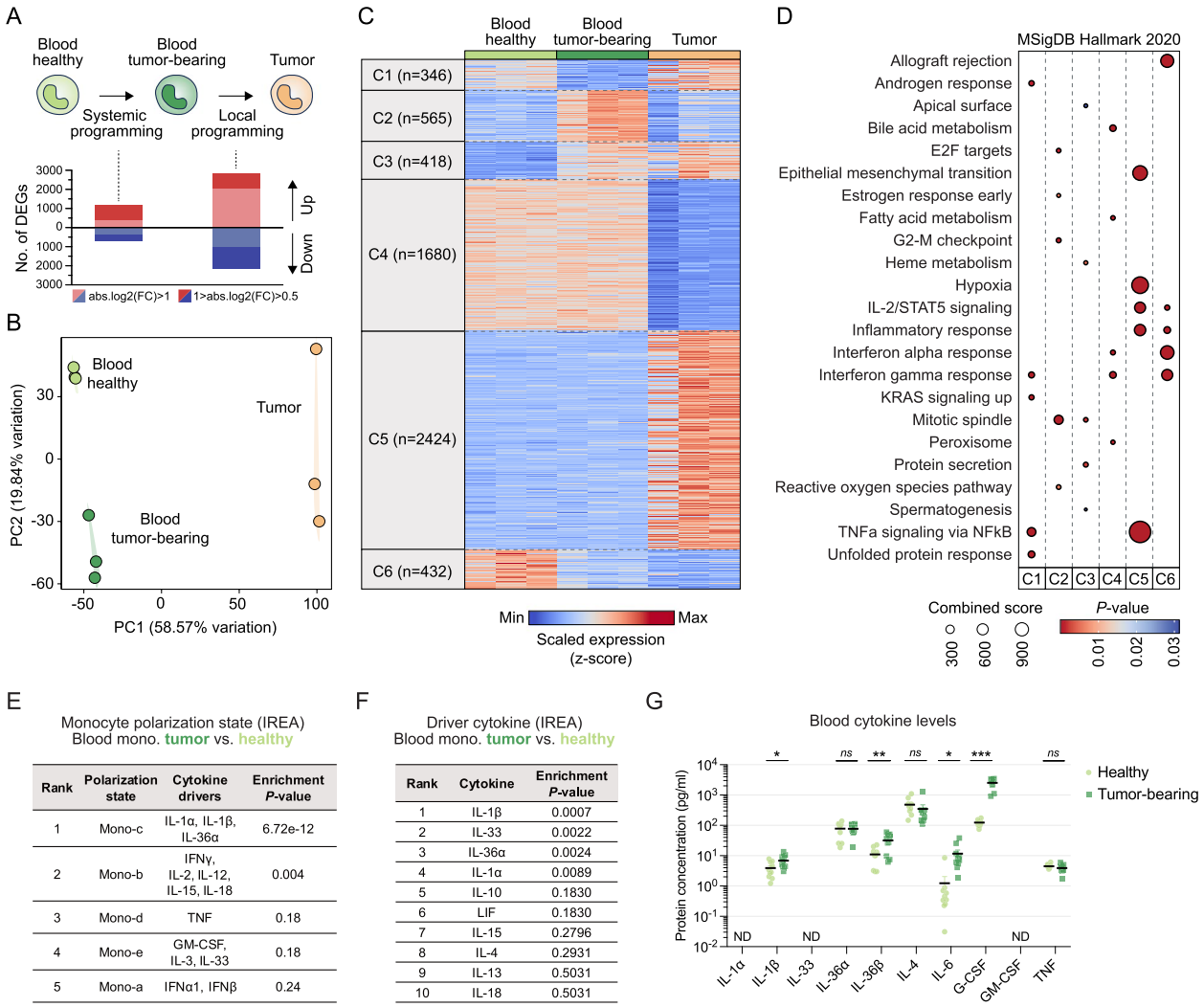

E

Rank	Polarization state	Cytokine drivers	Enrichment *P*-value
1	Mono-c	IL-1α, IL-1β, IL-36α	6.72e-12
2	Mono-b	IFNγ, IL-2, IL-12, IL-15, IL-18	0.004
3	Mono-d	TNF	0.18
4	Mono-e	GM-CSF, IL-3, IL-33	0.18
5	Mono-a	IFNα1, IFNβ	0.24

F

Rank	Cytokine	Enrichment *P*-value
1	IL-1β	0.0007
2	IL-33	0.0022
3	IL-36α	0.0024
4	IL-1α	0.0089
5	IL-10	0.1830
6	LIF	0.1830
7	IL-15	0.2796
8	IL-4	0.2931
9	IL-13	0.5031
10	IL-18	0.5031

Fig. 1 Tumor-induced systemic inflammation is associated with transcriptional preconditioning of peripheral monocytes. **A** Experimental scheme to examine peripheral and local programming of monocytes by the tumor and bar graphs showing the number of differentially expressed genes (DEGs) for the indicated comparisons, with different absolute log2(fold change) value thresholds. **B** Principal-component analysis of RNA-seq profiles of Ly6C^{hi} monocytes sorted from the blood of healthy mice, blood of LLC tumor-bearing mice and LLC tumors ($n = 3$). **C** Heatmap showing genes that were differentially expressed in at least one comparison between different conditions ($P < 0.05$ and absolute log2[fold change] ≥ 0.5), and separated into six clusters by *k*-means clustering. **D** Enrichment of MSigDB Hallmark gene sets in the different gene expression clusters. Top 5 enriched gene sets are shown for each cluster based on combined score. **E** Table showing the enrichment of different monocyte polarization states when compared to the upregulated genes in peripheral monocytes from tumor-bearing mice (log2FC > 0.5, FDR < 0.05) we identified, determined by the Immune Response Enrichment Analysis (IREA) algorithm. **F** Table showing the enrichment of different cytokine-induced transcriptome profiles when compared to the upregulated genes in peripheral monocytes from tumor-bearing mice, determined by the Immune Response Enrichment Analysis (IREA) algorithm. **G** Plasma levels of different pro-inflammatory cytokines in LLC tumor-bearing and healthy mice ($n = 9$–10/group, unpaired *t*-test, $^{*}P < 0.05$,$^{**}P < 0.01$, $^{***}P < 0.001$; ns, not significant; ND, not detected)

the differential genes in peripheral monocytes overlapped with differential transcripts previously identified in myeloid progenitors from tumor-bearing mice [37], suggesting that at least some of the transcriptomic changes in peripheral monocytes likely originated in monocyte precursors in the bone marrow (Additional file 1: Fig. S2, Additional file 2: Table S1).

Differentially expressed genes ($P < 0.05$ and absolute log2[fold change] ≥ 0.5) could be split into six major clusters with distinct gene expression patterns (Fig. 1C, Additional file 3: Table S2). This approach enabled us to identify two gene clusters (Clusters 3 and 6) whose expression was modulated in the periphery in tumor-bearing mice, and these alterations persisted following

tumor infiltration. Cluster 3 included genes whose expression was induced by the tumor in peripheral monocytes, and their expression level remained elevated following tumor infiltration. Similarly, Cluster 6 included genes whose expression was repressed in blood monocytes of tumor-bearing mice and remained repressed following tumor infiltration. We also identified gene clusters (Clusters 1 and 2) whose expression was altered in peripheral monocytes in response to the distal tumor, but this was reversed upon tumor infiltration. Finally, we found two large gene clusters (Clusters 4 and 5) whose expression did not show major differences in the blood but showed marked down- or upregulation during blood-to-tumor transition.

In order to link functional gene programs to these gene expression clusters, we analyzed the enrichment of Hallmark gene sets (Fig. 1D). Genes induced in peripheral monocytes of tumor-bearing mice (Clusters 2 and 3) showed specific enrichment of proliferation-related gene sets ("G2-M checkpoint," "Mitotic spindle," "E2F targets"), suggesting enhanced monocyte production in response to the tumor, in line with the observed increase in systemic monocyte levels (Additional file 1: Fig. S1A). Cluster 3 genes, which were induced by the tumor in the periphery and remained induced within the tumor, also included genes related to protein secretion and heme metabolism, the latter being an important driver of macrophage reprogramming in tumors [38–40]. Genes that were only turned on upon tumor infiltration (Cluster 5) showed specific enrichment for gene sets related to inflammation and the hypoxia response, indicating local activation and adaptation to the tumor microenvironment. We found that the gene cluster repressed upon tumor infiltration (Cluster 4) was enriched for interferon response genes. Interestingly, however, interferon response-related genes showed the strongest enrichment in the gene cluster which was already repressed in the periphery and remained repressed following tumor infiltration (Cluster 6).

These transcriptomic changes in monocytes were associated with a gradual increase in their T-cell suppressive activity ranging from blood monocytes from healthy mice, through blood monocytes from tumor-bearing mice, to tumor-infiltrating monocytes (Additional file 1: Fig. S3A,B). In contrast, the ability of monocytes to support cancer cell proliferation was not altered appreciably by the tumor, neither systemically nor locally (Additional file 1: Fig. S3C).

By comparing our data to previously published monocyte polarization states [31], we found a highly significant enrichment of an IL-1-driven transcriptional program in peripheral monocytes from tumor-bearing hosts (Fig. 1E, F). Accordingly, analysis of pro-inflammatory cytokines in the blood of tumor-bearing mice revealed significantly higher levels of IL-1 family cytokines IL-1β and IL-36β, along with IL-6 and the IL-1β-dependent cytokine G-CSF (Fig. 1G) [41].

Overall, these results demonstrate that the transcriptome of Ly6C^{hi} monocytes undergoes major changes upon tumor infiltration. However, peripheral monocytes in tumor-bearing mice already show transcriptomic alterations, which could be linked to systemic tumor-associated inflammation. Tumor-induced changes in the expression of specific gene sets in peripheral monocytes, including those related to interferon response, persist following tumor infiltration, suggesting a tumor-driven preconditioning of monocytes impacting their transcriptional program within the tumor.

Tumor-induced epigenetic alterations at promoters in peripheral monocytes lead to repression of interferon-responsive promoters and activation of pro-tumoral genes

Our observation that some genes in peripheral blood monocytes showed durable expression changes in the tumor-bearing state suggested that some of these genes were programmed at the epigenetic level in the periphery, making their transcriptional induction or repression more stable in the tumor.

In order to detect potential tumor-induced epigenomic alterations in monocytes, we first assessed the genome-wide distribution of Histone H3 Lysine 4 trimethylation (H3K4me3), a key histone modification for transcriptional initiation characteristic of promoter regions [42], using the CUT&Run method. We detected H3K4me3 signal predominantly (88%) at or near promoter regions, as expected (Additional file 1: Fig. S4). Comparative analysis between blood monocytes from LLC tumor-bearing and healthy mice revealed a set of promoters with altered H3K4me3 signal (166 induced and 312 repressed sites with $P < 0.05$, absolute log2[fold change] ≥ 0.5) (Fig. 2A, B, Additional file 4: Table S3).

By linking the nearest gene to each changing promoter, we found that genes with induced promoters were related to cellular functions such as cell division (e.g., *Cdk1*, *Cdkn1a*, *Plk1*), cell adhesion and migration (e.g., *Rhov*, *F11r*), and immunosuppression (e.g., *Socs3*, *Siglece*, *Cd38*). Among the genes with repressed promoters, we found several genes linked to the interferon response (e.g., *Ifit206*, *Rsad2*, *Mx2*) (Fig. 2A). These observations were further supported by the significant enrichment of the corresponding Hallmark gene sets related to cell division and the interferon response among the genes with induced and repressed promoters, respectively (Fig. 2C).

While no known motifs were significantly enriched among induced promoters, we found significant

enrichment of interferon-responsive IRF and ISRE motifs among repressed promoters (Fig. 2D). In line with these data, nearly all IRF transcription factor family members, except for *Irf9,* showed significantly reduced expression in peripheral monocytes of tumor-bearing mice, with *Irf1* and *Irf7* showing the greatest downregulation (Additional file 1: Fig. S5).

We then performed ATAC-seq to map chromatin accessibility across the genome of blood monocytes from healthy and LLC tumor-bearing mice and used these data to compare chromatin accessibility specifically at differential promoters. This analysis showed that average chromatin accessibility slightly decreased at repressed promoters in tumor-bearing mice (Fig. 2E). In addition, promoters that were induced by the tumor showed higher chromatin accessibility already at baseline in healthy mice, and accessibility at these sites did not increase further in response to the tumor (Fig. 2E).

In order to obtain information about promoter activity, we used CUT&Tag to analyze the genome-wide distribution of Histone H3 Lysine 27 acetylation (H3K27ac), a histone modification characteristic of promoters and enhancers with active transcription [43–46]. Similar to chromatin accessibility, promoters that were induced in tumor-bearing mice already showed higher average H3K27ac signal in healthy mice compared to repressed promoters, indicating higher baseline activity. In addition, the H3K27ac signal was further enhanced on this set of promoters in response to the distal tumor (Fig. 2E).

Next, we asked whether genes with differential promoters showed changes in their expression either in the blood or upon tumor infiltration and, if so, which previously identified gene expression cluster (shown in Fig. 1C) they can be linked to. Remarkably, less than half of the genes with altered promoters showed expression changes in the blood or upon tumor infiltration, indicating that promoter alterations were not necessarily associated with a direct change in transcription (Fig. 2F). Among the genes where promoter reprogramming could be linked to transcriptional change, we found that genes induced in the circulation (Clusters 2 and 3 in Fig. 1C) could be almost exclusively linked to induced promoters (Fig. 2G). Such epigenetically programmed genes included *Cd38* and *Trem2*, which have well-established roles in driving immunosuppressive and pro-tumoral functions of monocytes/macrophages [47–54]. These genes showed increased H3K4me3 at their promoters in the circulating monocytes from tumor-bearing mice, and this was associated with a persistently enhanced transcription upon tumor infiltration (Fig. 2H, I). Similarly, repressed genes in the circulation (Clusters 1 and 6 in Fig. 1C) could only be linked to repressed promoters (Fig. 2G), further indicating a close correspondence between the direction of changes in promoter H3K4me3 levels and in gene expression. Such repressed genes included *Slamf8*, a negative regulator of ROS production, and *Clec12a*, an inhibitory receptor involved in cell death sensing (Fig. 2J, K) [55, 56].

Interestingly, genes that were upregulated only upon tumor infiltration (Cluster 5 in Fig. 1C) could be preferentially linked to promoters induced in the circulation (Fig. 2G). This raised the possibility that tumor-induced epigenetic changes at promoters could prime genes for activation upon tumor infiltration. This gene set included *Socs3*, *Thbs1*, and *Myc*, which have been previously linked to immunosuppressive and tumor-promoting functions in macrophages (Fig. 2L, M, Additional file 1: Fig. S6) [57–60].

Overall, these data indicate that a set of promoters exhibit tumor-induced alterations in monocytes prior to tumor infiltration. This involves the repression of interferon-responsive promoters and the potential priming of key pro-tumoral genes for expression in the tumor microenvironment.

(See figure on next page.)

Fig. 2 Tumor-induced epigenetic alterations at promoters in peripheral monocytes lead to repression of interferon-responsive promoters and activation of pro-tumoral genes. **A** Volcano plot showing genomic sites with differential H3K4me3 signal between Ly6C^{hi} monocytes from the blood of LLC tumor-bearing versus healthy mice ($P < 0.05$ and absolute log2[fold change] ≥ 0.5). Representative closest protein-coding genes are highlighted. **B** Read distribution plot showing H3K4me3 signal at genomic sites with differential H3K4me3 signal. **C** Enrichment of MSigDB Hallmark gene sets among genes annotated to genomic sites with differential H3K4me3 signal. Top 5 gene sets are shown by *p*-value. **D** Top 5 known transcription factor (TF) motifs enriched among genomic sites showing repressed H3K4me3 signal in Ly6C^{hi} monocytes from the blood of LLC tumor-bearing mice versus healthy mice. **E** Chromatin accessibility (ATAC-seq) and H3K27ac signal in Ly6C^{hi} monocytes from the blood of healthy and LLC tumor-bearing mice at genomic sites with repressed or induced H3K4me3 signal when comparing tumor-bearing vs. healthy. Boxes show the median and the interquartile range (IQR), whiskers show highest and lowest values within 1.5 × IQR. Wilcoxon test; ns: not significant, *$P < 0.05$, **$P < 0.01$, ***$P < 0.001$. **F** Frequency of genes with differential H3K4me3 signal that are among the differentially expressed genes identified in Fig. 1C (DEG) or not (non-DEG). **G** Frequency of different cluster identities (determined in Fig. 1C) among the genes with induced or repressed H3K4me3 signal. **H**–**M** Genome browser snapshots showing average H3K4me3 signal in Ly6C^{hi} monocytes from the blood of healthy and LLC tumor-bearing mice at representative genes from different expression clusters. Bar plots show mRNA expression of the same genes determined by RNA-seq. Bar plots show mean + SEM

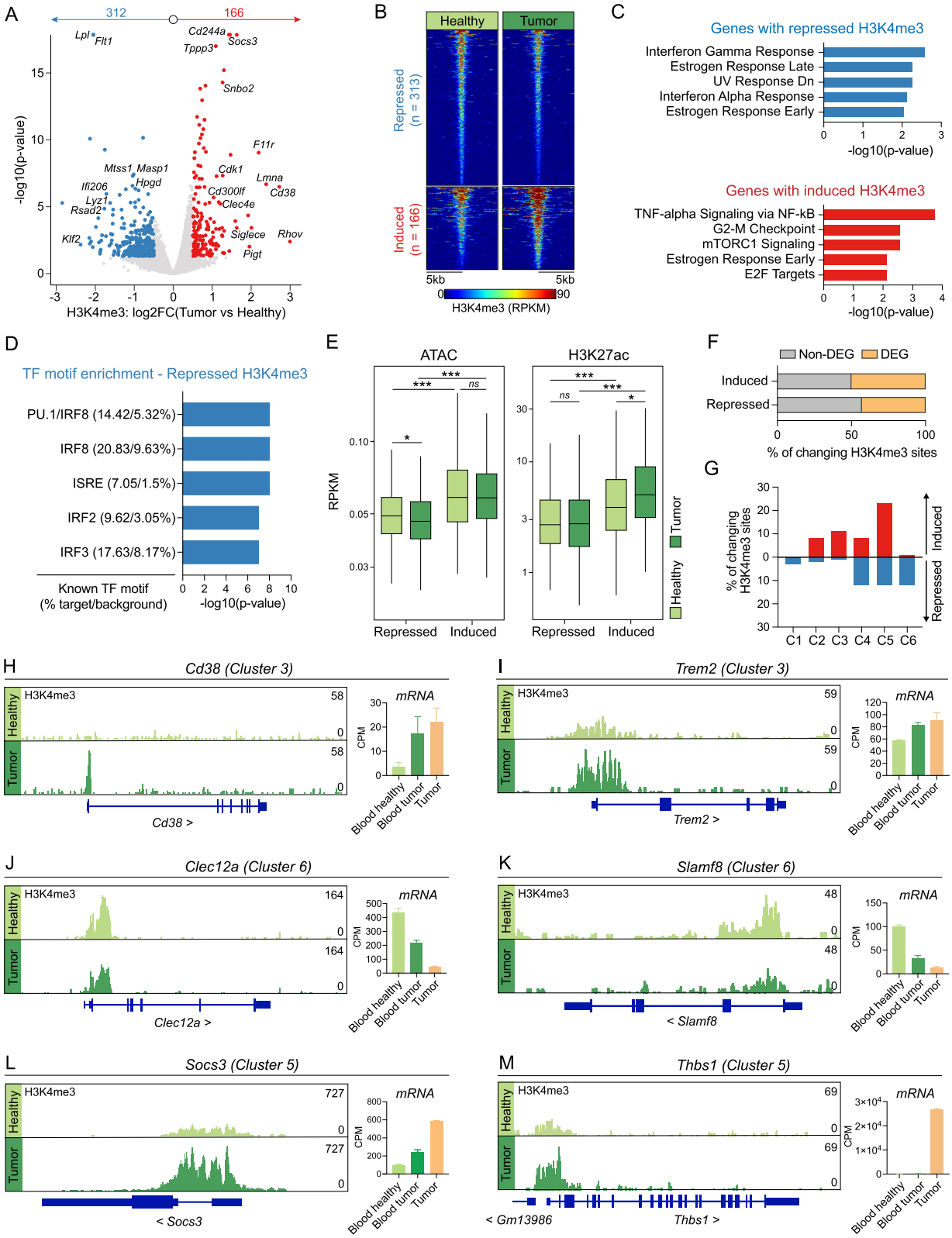

Fig. 2 (See legend on previous page.)

The enhancer landscape in peripheral monocytes is remodeled in response to the tumor, affecting a distinct set of transcription factor binding motifs

We hypothesized that enhancers of peripheral monocytes may also show changes in response to the distal tumor. Hence, we used CUT&Tag to analyze the enhancer landscape of peripheral monocytes from healthy and LLC tumor-bearing mice by assaying the genome-wide distribution of histone H3 Lysine 4 monomethylation (H3K4me1), a histone modification which marks enhancers [61].

Differential analysis between peripheral monocytes from tumor-bearing and healthy mice revealed more than 3000 genomic regions with altered H3K4me1 signal, which represented approximately 10% of all detected H3K4me1$^+$ enhancers (1757 induced and 1427 repressed sites at $P < 0.05$, absolute log2[fold change] ≥ 0.5 among 33,110 total detected H3K4me1$^+$ regions) (Fig. 3A, B, Additional file 5: Table S4). Most of these tumor-modulated enhancers were located in distal intergenic regions or introns (Fig. 3C).

Average chromatin accessibility significantly decreased at repressed enhancers, whereas it increased at induced enhancers, indicating chromatin remodeling at these sites (Fig. 3D). Average H3K27ac levels significantly increased at induced enhancers in tumor-bearing mice, indicating elevated enhancer activity, whereas H3K27ac levels remained unaltered at repressed enhancers (Fig. 3D).

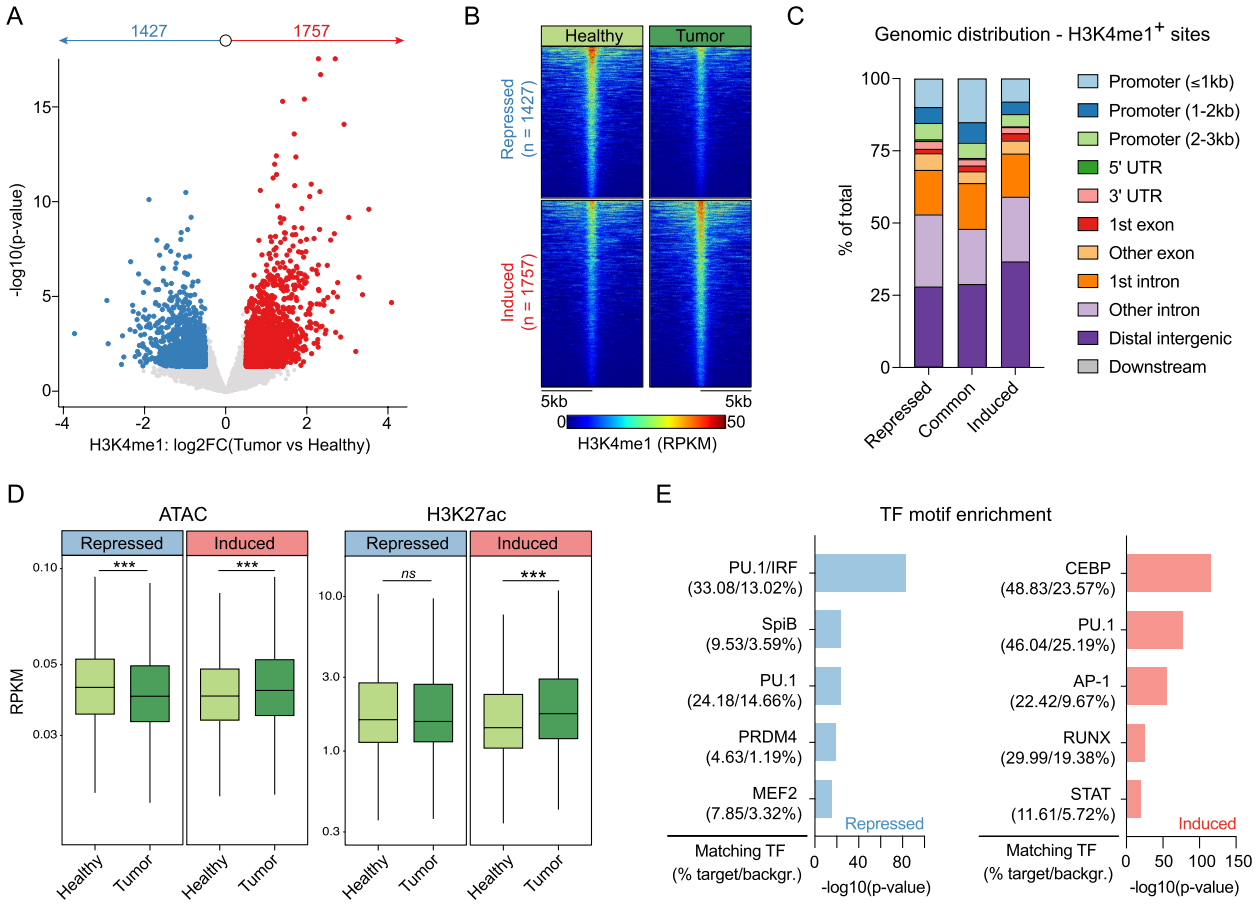

Fig. 3 The enhancer landscape in peripheral monocytes is remodeled in response to the tumor, affecting a distinct set of transcription factor binding motifs. **A** Volcano plot showing genomic sites with differential H3K4me1 signal between Ly6C^{hi} monocytes from the blood of LLC tumor-bearing versus healthy mice ($P < 0.05$ and absolute log2[fold change] ≥ 0.5). **B** Read distribution plot showing H3K4me1 signal at genomic sites with differential H3K4me1 signal. **C** Genomic distribution of sites with differential and unaltered H3K4me1 signal. **D** Chromatin accessibility (ATAC-seq) and H3K27ac signal in Ly6C^{hi} monocytes from the blood of healthy and LLC tumor-bearing mice at genomic sites with repressed or induced H3K4me1 signal when comparing tumor-bearing vs. healthy. Boxes show the median and the interquartile range (IQR), whiskers show highest and lowest values within 1.5 × IQR. Wilcoxon test; ns: not significant, ***$P < 0.001$. **E** Top 5 transcription factors (TF) matched to de novo motifs enriched among genomic sites showing repressed or induced H3K4me1 signal in Ly6C^{hi} monocytes from the blood of LLC tumor-bearing mice vs. healthy mice. De novo motif sequences and similarity scores to matched known motifs are shown in Figure S7

Transcription factor motif enrichment analysis on differential enhancers revealed enrichment of the PU.1 motif both at repressed and induced sites (Fig. 3E, Additional file 1: Fig. S7). This was expected, as PU.1 is a myeloid lineage-determining factor which has an essential role in maintaining cell type-specific enhancers [21]. Among the repressed enhancers, we found strong enrichment of the PU.1-IRF composite motif, adding further support to the notion that IRF activity is suppressed in peripheral monocytes in response to the tumor (Fig. 3E). Among the induced enhancers, the most significantly enriched motifs could be linked to C/EBP, AP-1, RUNX, and STAT transcription factor families, all of which can mediate response to extracellular inflammatory signals and cytokines (Fig. 3E). Expression levels of transcription factors belonging to these families were largely unaltered in peripheral monocytes, but many of them showed marked upregulation following tumor infiltration (Additional file 1: Fig. S8A). In line with this, gene regulatory network inference based on transcriptomic data revealed high inferred activities in tumor-infiltrating monocytes for C/EBPβ, multiple AP-1 members (e.g., FOS, JUN) and STAT3, whereas no marked tumor-induced changes could be observed in peripheral monocytes in the activity of these transcription factors (Additional file 1: Fig. S8B, Additional file 6: Table S5).

Altogether these results indicate that a distal tumor is able to remodel the enhancer landscape in peripheral monocytes. Specifically, this involves repression of enhancers capable of binding interferon-responsive IRF transcription factors as well as the establishment of enhancers harboring motifs for transcription factor families that can be activated by inflammatory and cytokine signaling, including C/EBP, AP-1, and STAT.

Remodeled enhancers in peripheral monocytes are linked to lasting gene expression programs and to subsequent gene activation in the tumor microenvironment

Finally, we sought to link differential enhancers to genes modulated by the tumor either in the periphery or upon tumor infiltration. To this end, we analyzed the frequency of induced and repressed enhancers in a ± 100 kilobase (kb) window around the transcription start site of differentially expressed genes belonging to different clusters described in Fig. 1C (Fig. 4A). The observed enhancer frequencies were then compared to enhancer frequencies detected around random gene sets of the same size, in order to determine the enrichment or depletion of differential enhancers around distinct gene clusters (Fig. 4A). This analysis revealed the strongest enrichment of induced and repressed enhancers around the previously defined C3 and C6 gene expression clusters, respectively (Fig. 4B, Additional file 1: Fig. S9). These clusters comprised genes that showed induction or repression in the periphery, which persisted following tumor infiltration (e.g., *Hebp1* and *Soat2* from C3; *Ifi27l2a* and *Tlr11* from C6, Fig. 4C–F). Interestingly, genes whose peripheral activation or inhibition could be reversed in the tumor (C2 and C1, respectively) did not show such a strong association with altered enhancers (Fig. 4B, Additional file 1: Fig. S9). Notably, genes that were only induced in the tumor microenvironment (C5) showed a marked enrichment of induced enhancers and a significant depletion of repressed enhancers in their vicinity (e.g., *Nos2* and *Rhov*, Fig. 4B, G, H, Additional file 1: Fig. S9). In addition, we also found significant enrichment of repressed enhancers but no depletion of induced enhancers, around genes which were downregulated upon tumor infiltration (C4) (Fig. 4B, Additional file 1: Fig. S9).

The association of induced enhancers with C5 genes indicated that a large number of genes that are induced upon tumor infiltration show increased H3K4me1 in their vicinity in response to the tumor already in the

(See figure on next page.)

Fig. 4 Remodeled enhancers in peripheral monocytes are linked to lasting gene expression programs and to subsequent gene activation in the tumor microenvironment. **A** Scheme summarizing the approach to determine enrichment of differential enhancers (increased or decreased H3K4me1 signal in tumor-bearing mice) ± 100 kilobase (kb) around the transcription start site of differentially expressed genes (DEGs) identified in Fig. 1C. **B** Fold change and *z*-test *p*-value of the comparison of the number of differential enhancers found ± 100 kb around genes belonging to the indicated expression clusters versus random gene sets of the same sizes. The number of differential enhancers found for each cluster and the corresponding random gene sets are shown in Fig. S9. **C**–**H** Genome browser snapshots showing average H3K4me1 signal in Ly6C^{hi} monocytes from the blood of healthy and LLC tumor-bearing mice at representative genes from different expression clusters. Bar plots show mRNA expression of the same genes determined by RNA-seq. Bar plots show mean + SEM. **I** Cartoon showing analysis method for motif enrichment at enhancer sets linked to C3 and C5 gene clusters defined in Fig. 1C. **J** Heatmap showing transcription factor binding motifs with significant enrichment at induced enhancers linked to either Cluster 3 (C3) or Cluster 5 (C5) ($n = 91$ enhancers linked to C3, $n = 431$ enhancers linked to C5, HOMER known motifs, FDR < 0.05). **K** Heatmap showing enrichment of different STAT transcription factor motifs from the JASPAR motif collection to either C3 or C5 genes ($n = 91$ enhancers linked to C3, $n = 431$ enhancers linked to C5, motifs with FDR < 0.05 are shown in bold; monaLisa motif enrichment analysis)

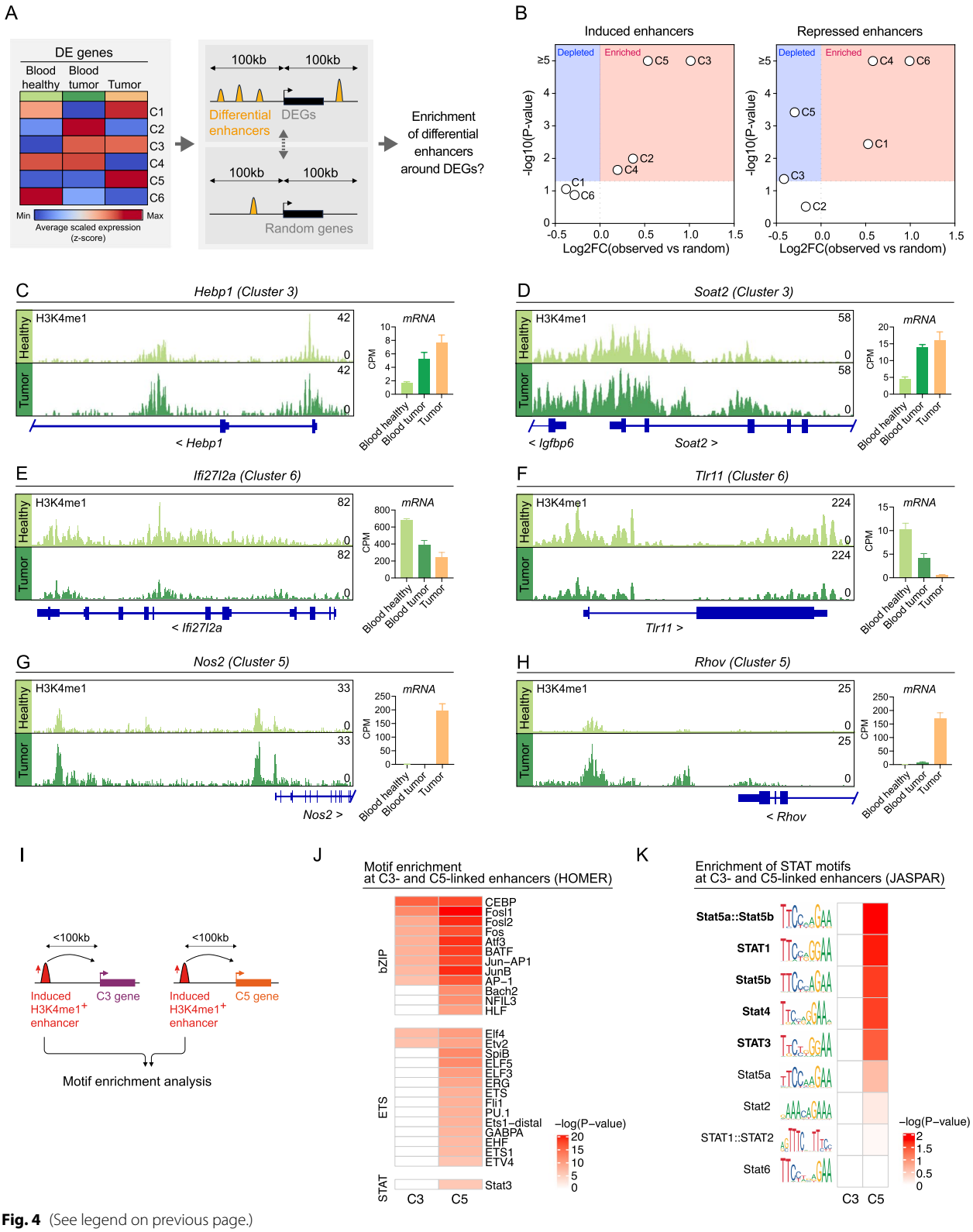

Fig. 4 (See legend on previous page.)

circulation. To further examine these genes and their associated enhancers, we linked induced H3K4me1$^+$ enhancers to nearby C5 genes (< 100 kb). We found that a subset of these genes showed slightly but significantly increased transcription already in the periphery (Additional file 1: Fig. S10), but the majority of them was not altered.

In order to determine whether C5-associated enhancers contain distinct transcription factor binding motifs compared to enhancers linked to C3 genes (induced already in periphery), we performed motif enrichment analysis on these two enhancer sets (Fig. 4I). We found that both C3- and C5-associated enhancers showed enrichment of C/EBP, AP-1, and ETS-related transcription factor motifs (Fig. 4J) with C3-linked enhancers exhibiting the strongest enrichment for C/EBP motifs. Notably, STAT motif enrichment could only be detected at enhancers associated with C5 genes. Specific enrichment of STAT motifs at C5-linked enhancers was further confirmed by an independent approach, using the monaLisa enrichment tool with the JASPAR motif database (Fig. 4K).

We also performed motif enrichment analysis on repressed H3K4me1$^+$ enhancers which could be linked to Cluster 6 genes (genes with durable repression maintained in the tumor). This analysis revealed significant enrichment of SpiB, PU.1 and PU.1–IRF motifs (Additional file 1: Fig. S11), which corresponded to the three most significantly enriched motifs we previously found when considering all repressed H3K4me1$^+$ enhancers (Fig. 3E).

Overall, these results indicate that altered enhancers are enriched primarily around genes with peripheral gene expression changes that persist throughout the blood-to-tumor transition of monocytes. This suggests that epigenomic alterations can instruct sustained gene expression changes that are less likely to be reversed in the tumor microenvironment. In addition, strong enrichment of enhancers induced in the periphery around genes activated upon tumor infiltration suggests an epigenetic priming effect at these loci.

Discussion

This study provides proof-of-principle evidence in mice for tumor-induced peripheral epigenomic alterations in monocytes and their association with gene expression changes occurring before and after tumor infiltration. Specifically, our results suggest a model whereby epigenomic programming in the periphery can shape the monocyte transcriptome in multiple ways (Fig. 5). First, activation of promoters and/or enhancers in peripheral monocytes can initiate transcription in the periphery and maintain gene expression following tumor infiltration. Second, repression of promoters and/or enhancers

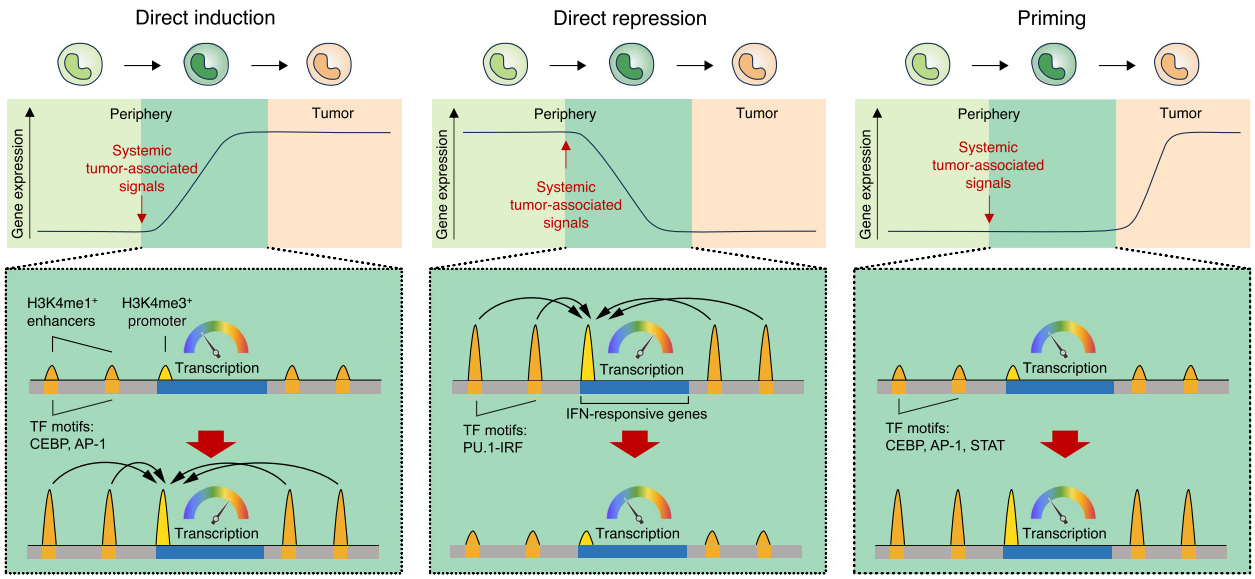

Fig. 5 Graphical summary showing the proposed model of different ways by which tumor-induced epigenomic preconditioning can alter gene expression in monocytes. Genes with direct induction show activation of the promoter and/or nearby enhancers in the periphery. This is associated with increased transcription in the periphery that persists upon tumor infiltration. Genes with direct repression show the opposite pattern: a repressed promoter and/or nearby enhancers are associated with durable repression of gene transcription that persists following tumor infiltration. Epigenetic changes at promoters and/or enhancers may also prime genes for activation in the tumor microenvironment without causing major changes in gene expression in the periphery. Characteristic transcription factor (TF) motifs associated with each distinct enhancer set are indicated

in peripheral monocytes can lead to durable repression of gene expression (e.g., interferon-responsive genes), even after the cells infiltrate the tumor. Third, epigenetic changes at certain promoters and/or enhancers in peripheral monocytes can prime genes for activation within the tumor without causing major changes in gene expression in the periphery. The latter is likely due to the fact that transcriptional activation of these genes requires enhancer binding by transcription factors that are only activated in the tumor microenvironment. This model, particularly the proposed epigenomic priming mechanism, will require further experimental validation. Future studies should assess whether perturbing upstream pathways and epigenetic regulators driving deposition of histone marks at potentially primed genes could impair gene induction upon tumor infiltration.

We observed that peripheral epigenomic programming of monocytes by the distant tumor involves repression of interferon-responsive promoters and enhancers harboring IRF and ISRE motifs. These findings are in line with previous observations of a suppressed interferon response of peripheral monocytes in cancer patients [16–18, 62]. Our results suggest that epigenetic repression of interferon-responsive promoters and enhancers could represent one possible mechanism by which the systemic influence of a tumor desensitizes monocytes to immunostimulatory interferons and thereby suppresses anti-tumor immunity.

By integrating data on peripheral epigenomic changes and the transcriptional response during blood-to-tumor transition of monocytes, we found that genes activated in the tumor microenvironment associate with enhancers that are already induced in the periphery in response to the tumor. Generally, establishment of the enhancer repertoire is governed by lineage-specific differentiation programs and prior stimuli received by the cell [21]. In macrophages, pre-established enhancers are the dominant genomic sites where signal-dependent transcription factors, such as NF-κB, AP-1, and STAT members, can bind the DNA and activate transcription in response to microenvironmental stimuli [21]. Our results indicate that new H3K4me1^{+} enhancers harboring binding motifs for signal-dependent transcription factors, including AP-1 and STAT, are established in peripheral monocytes in response to the distal tumor. An important consequence of this may be an amplified transcriptional response to signals that activate these transcription factors upon tissue infiltration. We observed that the expression levels and inferred activities of several key transcription factors (e.g., C/EBPβ, AP-1, STAT3) increase following tumor infiltration, which could further facilitate the activation of pre-established enhancers containing their binding motifs. It will be important to investigate to what extent such remodeling of the enhancer landscape prior to tumor infiltration can bias monocyte fate and macrophage polarity in the tumor through altering the transcriptional response to the microenvironment.

This study adds support to the emerging notion that systemic immune perturbations induced by tumor-associated signals can influence localized responses to the tumor [63]. Specifically, our work uncovers epigenomic programming of monocytes as a previously unexplored tumor-induced systemic immune perturbation. This observation opens up several important avenues for possible future investigation.

It remains to be elucidated which of these changes are established already during monocyte development and at which stage of differentiation. This will require genome-wide analysis of different histone modifications, chromatin accessibility, and transcriptome in multiple different progenitor populations along the monocyte differentiation trajectory.

It will be also important to identify how systemic tumor-associated signals drive this process. Our computational predictions and blood cytokine measurements nominated IL-1 family cytokines (IL-1β and IL-36β) as key drivers of the observed transcriptomic changes in peripheral monocytes. This is in line with recent findings about the role of IL-1β in the systemic programming of pro-tumor neutrophils [37]. In addition, we found elevated circulating levels of IL-6 and G-CSF in tumor-bearing mice, which could contribute to the observed preconditioning of monocytes. Correspondingly, downstream transcription factors linked to these cytokines showed motif enrichment at induced enhancers in tumor-bearing mice (AP-1 for IL-1 [64], C/EBPβ for G-CSF [65], STAT3 for IL-6 [66]). Further studies involving proteomics and metabolomics analyses to detect tumor-associated signals, followed by in vivo perturbations of candidate pathways combined with epigenomic and transcriptomic profiling of monocytes, will likely yield valuable insights into the causal role of specific signals. Tumor-derived factors reaching the systemic circulation are often dictated by the specific genetic alterations of a tumor [67]. Hence, it will be interesting to determine to what extent epigenomic programming and its drivers are specific for each tumor type.

A limitation of the current study is the lack of epigenomic data from tumor-infiltrating monocytes. Hence, detailed analysis of the epigenomic landscape upon tumor infiltration of monocytes, particularly at genes with features of epigenetic priming, will require further investigation.

This work also paves the way for future studies, which should assess epigenomic alterations in peripheral

monocytes in cohorts of cancer patients. Such studies could potentially identify novel epigenetic biomarkers for diagnosis and disease follow-up.

Conclusions

Overall, this study identifies the epigenomic landscape as a regulatory layer disrupted in peripheral monocytes by the systemic effects of a tumor. Our results suggest that this epigenomic preconditioning is important both in establishing lasting gene expression programs in monocytes prior to tumor infiltration and in shaping their subsequent transcriptional response to the tumor microenvironment. These findings provide new insights into how the fate of monocytes is redirected to support cancer progression and position the monocyte epigenome as a potential future therapeutic target and biomarker.

Supplementary Information

The online version contains supplementary material available at https://doi.org/10.1186/s13073-025-01511-y.

Additional file 1: Fig. S1-S11.

Additional file 2: Table S1. List of overlapping DEGs (FDR < 0.05) between blood monocytes (LLC tumor vs healthy, from this study) and bone marrow progenitors (KEP tumor vs healthy, from Garner et al. 2025). Related to Fig. S2.

Additional file 3: Table S2. List of differentially expressed genes and their cluster identities. Related to Fig. 1.

Additional file 4: Table S3. List of differential H3K4me3 peaks. Related to Fig. 2.

Additional file 5: Table S4. List of differential H3K4me1 peaks. Related to Fig. 3.

Additional file 6: Table S5. TF activity scores in monocytes from different tissue sources based on decoupleR gene regulatory network inference. Related to Fig. S8.

Acknowledgements

The authors thank Mozes Sze and Lars Vereecke for help with cytokine measurements, and Susan M. Gasser, Mikael J. Pittet and Aleksandar Murgaski for critical input on the manuscript.

Authors' contributions

M. K. conceptualized and initiated the study and wrote the manuscript. M.K. and L. H. prepared the figures. M.K., D.L., L.N. and J. A.V.G. designed experiments. M.K., E.H., W.K.B., P.T., S.P. and R.M.B. performed experiments. A.D., J.B. and Y.E. provided technical assistance. L.H., D.K., A.G., L.M. and Y.S. performed computational analyses. B.D. and Z.C. provided critical input for research design, computational analyses and data interpretation. D.L., L.N. and J.A.V.G. obtained funding, supervised experiments and data analysis, and edited the manuscript. All authors read and approved the final manuscript.

Funding

E.H. is supported by a grant from FWO (12Y1922N). E.H. and J.A.V.G. are supported by Stichting tegen Kanker (F/2024/2625). D.L. and J.A.V.G. are supported by grants from FWO, Kom op Tegen Kanker, Stichting tegen Kanker, VIB, and Vrije Universiteit Brussel. Z.C. was supported by the National Research, Development and Innovation Office (2023–1.1.1-PIACI_FÓKUSZ-2024–00036, K145994) and the János Bolyai Research Scholarship of the Hungarian Academy of Sciences (BO/00594/22/8). L.N. is supported by the NIH HL170426 and AI185363. S.P. was supported by the project TKP2021-NKTA-34, which has been implemented with the support provided by the Ministry of Culture and Innovation of Hungary from the National Research, Development and Innovation Fund, financed under the TKP2021-NKTA funding scheme.
Fonds Wetenschappelijk Onderzoek,12Y1922N,Stichting Tegen Kanker,F/2024/2625,F/2024/2625,National Institutes of Health,HL170426,HL170426,National Research,Development and Innovation Office,TKP2021-NKTA-34,2023-1.1.1-PIACI_FÓKUSZ-2024-00036,K145994,János Bolyai Research Scholarship,BO/00594/22/8

Data availability

RNA-seq, ATAC-seq, CUT&Run and CUT&Tag datasets generated in this study are available at the NCBI GEO under accession number GSE268992: https://www.ncbi.nlm.nih.gov/geo/query/acc.cgi?acc=GSE268992. All other source data are available from the corresponding author upon request.

Declarations

Ethics approval and consent to participate

All animal experiments were approved by the Ethical Committee for Animal Experiments of the Vrije Universiteit Brussel (licenses 15–220-3 and 19–220-8).

Consent for publication

Not applicable.

Competing interests

B.D. is employed at Genentech Inc., South San Francisco, CA, USA and is a shareholder of Roche. All other authors have no competing interests to disclose.

Author details

[1]Myeloid Cell Immunology Lab, VIB Center for Inflammation Research, Brussels, Belgium. [2]Laboratory of Cellular and Molecular Immunology, Brussels Center for Immunology, Vrije Universiteit Brussel, Brussels, Belgium. [3]Laboratory of Dendritic Cell Biology and Cancer Immunotherapy, VIB Center for Inflammation Research, Brussels, Belgium. [4]Departments of Medicine and Biomedical Engineering, Johns Hopkins University School of Medicine, Institute for Fundamental Biomedical Research, Johns Hopkins All Children's Hospital, St. Petersburg, FL, USA. [5]Department of Biochemistry and Molecular Biology, Faculty of Medicine, University of Debrecen, Debrecen, Hungary. [6]Department of Oncology, Ludwig Institute for Cancer Research Lausanne, University of Lausanne, Lausanne, Switzerland. [7]Data Mining and Modeling for Biomedicine Group, VIB-UGent Center for Inflammation Research, Ghent, Belgium. [8]Department of Biomedical Molecular Biology, Faculty of Science, Ghent University, Ghent, Belgium. [9]Department of Applied Mathematics, Computer Science and Statistics, Ghent University, Ghent, Belgium. [10]Genentech, South San Francisco, CA, USA. [11]Institute of Genetics, Biological Research Centre, Eotvos Lorand Research Network, Szeged, Hungary. [12]Department of Immunology, Albert Szent-Györgyi Medical School, Faculty of Science and Informatics, University of Szeged, Szeged, Hungary. [13]Present Address: AGORA Cancer Research Center, Lausanne, Switzerland. [14]Present Address: Icahn School of Medicine at Mount Sinai, The Tisch Cancer Institute, New York, NY, USA.

Received: 8 September 2024 Accepted: 10 July 2025
Published online: 23 July 2025

References

1. Guilliams M, Mildner A, Yona S. Developmental and Functional Heterogeneity of Monocytes. Immunity. 2018;49:595–613.
2. Singhal S, Stadanlick J, Annunziata MJ, Rao AS, Bhojnagarwala PS, O'Brien S, et al. Human tumor-associated monocytes/macrophages and their regulation of T cell responses in early-stage lung cancer. Science Translational Medicine. 2019;11:eaat1500-16.
3. Olingy CE, Dinh HQ, Hedrick CC. Monocyte heterogeneity and functions in cancer. J Leukoc Biol. 2019;106:309–22.
4. Zilionis R, Engblom C, Pfirschke C, Savova V, Zemmour D, Saatcioglu HD, et al. Single-Cell Transcriptomics of Human and Mouse Lung Cancers

Reveals Conserved Myeloid Populations across Individuals and Species. Immunity. 2019;50:1317-1334.e10.
5. Azizi E, Carr AJ, Plitas G, Cornish AE, Konopacki C, Prabhakaran S, et al. Single-Cell Map of Diverse Immune Phenotypes in the Breast Tumor Microenvironment. Cell. 2018;174:1293-1308.e36.
6. Cheng S, Li Z, Gao R, Xing B, Gao Y, Yang Y, et al. A pan-cancer single-cell transcriptional atlas of tumor infiltrating myeloid cells. Cell. 2021;184:792-809.e23.
7. Kitamura T, Doughty-Shenton D, Cassetta L, Fragkogianni S, Brownlie D, Kato Y, et al. Monocytes Differentiate to Immune Suppressive Precursors of Metastasis-Associated Macrophages in Mouse Models of Metastatic Breast Cancer. Front Immunol. 2018;8:69–14.
8. Tadepalli S, Clements DR, Saravanan S, Hornero RA, Lüdtke A, Blackmore B, et al. Rapid recruitment and IFN-I–mediated activation of monocytes dictate focal radiotherapy efficacy. Sci Immunol. 2023;8:eadd7446.
9. Kwart D, He J, Srivatsan S, Lett C, Golubov J, Oswald EM, et al. Cancer cell-derived type I interferons instruct tumor monocyte polarization. Cell Rep. 2022;41: 111769.
10. Krieg C, Nowicka M, Guglietta S, Schindler S, Hartmann FJ, Weber LM, et al. High-dimensional single-cell analysis predicts response to anti-PD-1 immunotherapy. Nat Med. 2018;24:144–53.
11. Carroll TM, Chadwick JA, Owen RP, White MJ, Kaplinsky J, Peneva I, et al. Tumor monocyte content predicts immunochemotherapy outcomes in esophageal adenocarcinoma. Cancer Cell. 2023;41:1222-1241.e7.
12. Zemek RM, Chin WL, Fear VS, Wylie B, Casey TH, Forbes C, et al. Temporally restricted activation of IFNβ signaling underlies response to immune checkpoint therapy in mice. Nat Commun. 2022;13:4895.
13. Kroemer G, McQuade JL, Merad M, André F, Zitvogel L. Bodywide ecological interventions on cancer. Nat Med. 2023;29:59–74.
14. Kiss M, Caro AA, Raes G, Laoui D. Systemic Reprogramming of Monocytes in Cancer. Front Oncol. 2020;10:1399.
15. Robinson A, Burgess M, Webb S, Louwe PA, Ouyang Z, Skola D, et al. Systemic Influences of Mammary Cancer on Monocytes in Mice. Cancers. 2022;14:833.
16. Lin Y, Gustafson MP, Bulur PA, Gastineau DA, Witzig TE, Dietz AB. Immunosuppressive CD14+HLA-DRlow/− monocytes in B-cell non-Hodgkin lymphoma. Blood. 2011;117:872–81.
17. Wang L, Simons DL, Lu X, Tu TY, Avalos C, Chang AY, et al. Breast cancer induces systemic immune changes on cytokine signaling in peripheral blood monocytes and lymphocytes. EBioMedicine. 2020;52: 102631.
18. Ramos RN, Rodriguez C, Hubert M, Ardin M, Treilleux I, Ries CH, et al. CD163 +tumor-associated macrophage accumulation in breast cancer patients reflects both local differentiation signals and systemic skewing of monocytes. Clinical & Translational Immunology. 2020;9:891–918.
19. Cassetta L, Fragkogianni S, Sims AH, Swierczak A, Forrester LM, Zhang H, et al. Human Tumor-Associated Macrophage and Monocyte Transcriptional Landscapes Reveal Cancer-Specific Reprogramming, Biomarkers, and Therapeutic Targets. Cancer Cell. 2019;35:588-602.e10.
20. Hamm A, Prenen H, Delm WV, Matteo MD, Wenes M, Delamarre E, et al. Tumour-educated circulating monocytes are powerful candidate biomarkers for diagnosis and disease follow-up of colorectal cancer. Gut. 2016;65:990–1000.
21. Glass CK, Natoli G. Molecular control of activation and priming in macrophages. Nat Immunol. 2016;17:26–33.
22. Ivashkiv LB. Epigenetic regulation of macrophage polarization and function. Trends Immunol. 2013;34:216–23.
23. Czimmerer Z, Nagy L. Epigenomic regulation of macrophage polarization: Where do the nuclear receptors belong? Immunol Rev. 2023;317:152–65.
24. Kiss M, Lebegge E, Murgaski A, Damme HV, Kancheva D, Brughmans J, et al. Junctional adhesion molecule-A is dispensable for myeloid cell recruitment and diversification in the tumor microenvironment. Front Immunol. 2022;13:1003975.
25. Kiss M, Walle LV, Saavedra PHV, Lebegge E, Damme HV, Murgaski A, et al. IL1β Promotes Immune Suppression in the Tumor Microenvironment Independent of the Inflammasome and Gasdermin D. Cancer Immunol Res. 2021;9:309–23.
26. Ewels PA, Peltzer A, Fillinger S, Patel H, Alneberg J, Wilm A, et al. The nf-core framework for community-curated bioinformatics pipelines. Nat Biotechnol. 2020;38:276–8.
27. Dobin A, Davis CA, Schlesinger F, Drenkow J, Zaleski C, Jha S, et al. STAR: ultrafast universal RNA-seq aligner. Bioinformatics. 2013;29:15–21.
28. Patro R, Duggal G, Love MI, Irizarry RA, Kingsford C. Salmon provides fast and bias-aware quantification of transcript expression. Nat Methods. 2017;14:417–9.
29. Robinson MD, McCarthy DJ, Smyth GK. edgeR: a Bioconductor package for differential expression analysis of digital gene expression data. Bioinformatics. 2010;26:139–40.
30. Kuleshov MV, Jones MR, Rouillard AD, Fernandez NF, Duan Q, Wang Z, et al. Enrichr: a comprehensive gene set enrichment analysis web server 2016 update. Nucleic Acids Res. 2016;44:W90–7.
31. Cui A, Huang T, Li S, Ma A, Pérez JL, Sander C, et al. Dictionary of immune responses to cytokines at single-cell resolution. Nature. 2024;625:377–84.
32. Badia-i-Mompel P, Santiago JV, Braunger J, Geiss C, Dimitrov D, Müller-Dott S, et al. decoupleR: ensemble of computational methods to infer biological activities from omics data. Bioinform Adv. 2022;2:vbac016.
33. Buenrostro JD, Giresi PG, Zaba LC, Chang HY, Greenleaf WJ. Transposition of native chromatin for fast and sensitive epigenomic profiling of open chromatin, DNA-binding proteins and nucleosome position. Nat Methods. 2013;10:1213–8.
34. Zhang Y, Liu T, Meyer CA, Eeckhoute J, Johnson DS, Bernstein BE, et al. Model-based analysis of ChIP-Seq (MACS). Genome Biol. 2008;9:R137.
35. Wang Q, Li M, Wu T, Zhan L, Li L, Chen M, et al. Exploring Epigenomic Datasets by ChIPseeker. Curr Protoc. 2022;2: e585.
36. Machlab D, Burger L, Soneson C, Rijli FM, Schübeler D, Stadler MB. monaLisa: an R/Bioconductor package for identifying regulatory motifs. Bioinformatics. 2022;38:2624–5.
37. Garner H, Martinovic M, Liu NQ, Bakker NAM, Velilla IQ, Hau C-S, et al. Understanding and reversing mammary tumor-driven reprogramming of myelopoiesis to reduce metastatic spread. Cancer Cell. 2025;43:1279-1295.e9.
38. Consonni FM, Bleve A, Totaro MG, Storto M, Kunderfranco P, Termanini A, et al. Heme catabolism by tumor-associated macrophages controls metastasis formation. Nat Immunol. 2021;22:595–606.
39. Alaluf E, Vokaer B, Detavernier A, Azouz A, Splittgerber M, Carrette A, et al. Heme oxygenase-1 orchestrates the immunosuppressive program of tumor-associated macrophages. JCI Insight. 2020;5:e133929.
40. Schaer DJ, Schulthess-Lutz N, Baselgia L, Hansen K, Buzzi RM, Humar R, et al. Hemorrhage-activated NRF2 in tumor-associated macrophages drives cancer growth, invasion, and immunotherapy resistance. J Clin Investig. 2024;134: e174528.
41. Coffelt SB, Kersten K, Doornebal CW, Weiden J, Vrijland K, Hau C-S, et al. IL-17-producing γδ T cells and neutrophils conspire to promote breast cancer metastasis. Nature. 2015;522:345–8.
42. Ruthenburg AJ, Allis CD, Wysocka J. Methylation of Lysine 4 on Histone H3: Intricacy of Writing and Reading a Single Epigenetic Mark. Mol Cell. 2007;25:15–30.
43. Heintzman ND, Hon GC, Hawkins RD, Kheradpour P, Stark A, Harp LF, et al. Histone modifications at human enhancers reflect global cell-type-specific gene expression. Nature. 2009;459:108–12.
44. Duttke SHC, Lacadie SA, Ibrahim MM, Glass CK, Corcoran DL, Benner C, et al. Human Promoters Are Intrinsically Directional. Mol Cell. 2015;57:674–84.
45. Chen FX, Smith ER, Shilatifard A. Born to run: control of transcription elongation by RNA polymerase II. Nat Rev Mol Cell Biol. 2018;19:464–78.
46. Calo E, Wysocka J. Modification of Enhancer Chromatin: What, How, and Why? Mol Cell. 2013;49:825–37.
47. Karakasheva TA, Dominguez GA, Hashimoto A, Lin EW, Chiu C, Sasser K, et al. CD38+ M-MDSC expansion characterizes a subset of advanced colorectal cancer patients. JCI Insight. 2018;3:99–109.
48. Karakasheva TA, Waldron TJ, Eruslanov E, Kim SB, Lee JS, O'Brien S, et al. CD38-Expressing Myeloid-Derived Suppressor Cells Promote Tumor Growth in a Murine Model of Esophageal Cancer. Can Res. 2015;75:4074–85.
49. Chen L, Diao L, Yang Y, Yi X, Rodriguez BL, Li Y, et al. CD38-Mediated Immunosuppression as a Mechanism of Tumor Cell Escape from PD-1/PD-L1 Blockade. Cancer Discov. 2018;8:1156–75.
50. Park MD, Reyes-Torres I, LeBerichel J, Hamon P, LaMarche NM, Hegde S, et al. TREM2 macrophages drive NK cell paucity and dysfunction in lung cancer. Nat Immunol. 2023;24:792–801.
51. Molgora M, Esaulova E, Vermi W, Hou J, Chen Y, Luo J, et al. TREM2 Modulation Remodels the Tumor Myeloid Landscape Enhancing Anti-PD-1 Immunotherapy. Cell. 2020;182:886-900.e17.

52. Katzenelenbogen Y, Sheban F, Yalin A, Yofe I, Svetlichnyy D, Jaitin DA, et al. Coupled scRNA-Seq and Intracellular Protein Activity Reveal an Immunosuppressive Role of TREM2 in Cancer. Cell. 2020;182:872-885.e19.
53. Sun R, Han R, McCornack C, Khan S, Tabor GT, Chen Y, et al. TREM2 inhibition triggers antitumor cell activity of myeloid cells in glioblastoma. Sci Adv. 2023;9:eade3559.
54. Binnewies M, Pollack JL, Rudolph J, Dash S, Abushawish M, Lee T, et al. Targeting TREM2 on tumor-associated macrophages enhances immunotherapy. Cell Rep. 2021;37: 109844.
55. Wang G, Abadía-Molina AC, Berger SB, Romero X, O'Keeffe MS, Rojas-Barros DI, et al. Cutting Edge: Slamf8 Is a Negative Regulator of Nox2 Activity in Macrophages. J Immunol. 2012;188:5829–32.
56. Neumann K, Castiñeiras-Vilariño M, Höckendorf U, Hannesschläger N, Lemeer S, Kupka D, et al. Clec12a Is an Inhibitory Receptor for Uric Acid Crystals that Regulates Inflammation in Response to Cell Death. Immunity. 2014;40:389–99.
57. Omatsu M, Nakanishi Y, Iwane K, Aoyama N, Duran A, Muta Y, et al. THBS1-producing tumor-infiltrating monocyte-like cells contribute to immunosuppression and metastasis in colorectal cancer. Nat Commun. 2023;14:5534.
58. Pello OM, Chèvre R, Laoui D, Juan AD, Lolo F, Andrés-Manzano MJ, et al. In Vivo Inhibition of c-MYC in Myeloid Cells Impairs Tumor-Associated Macrophage Maturation and Pro-Tumoral Activities. PLoS ONE. 2012;7: e45399.
59. Pello OM, Pizzol MD, Mirolo M, Soucek L, Zammataro L, Amabile A, et al. Role of c-MYC in alternative activation of human macrophages and tumor-associated macrophage biology. Blood. 2012;119:411–21.
60. Qin H, Holdbrooks AT, Liu Y, Reynolds SL, Yanagisawa LL, Benveniste EN. SOCS3 Deficiency Promotes M1 Macrophage Polarization and Inflammation. J Immunol. 2012;189:3439–48.
61. Black JC, Van Rechem C, Whetstine JR. Histone Lysine Methylation Dynamics: Establishment, Regulation, and Biological Impact. Mol Cell. 2012;48:491–507.
62. Verronèse E, Delgado A, Valladeau-Guilemond J, Garin G, Guillemaut S, Tredan O, et al. Immune cell dysfunctions in breast cancer patients detected through whole blood multi-parametric flow cytometry assay. Oncoimmunology. 2015;5: e1100791.
63. Hiam-Galvez KJ, Allen BM, Spitzer MH. Systemic immunity in cancer. Nat Rev Cancer. 2021;21:345–59.
64. Weber A, Wasiliew P, Kracht M. Interleukin-1 (IL-1) Pathway. Sci Signal. 2010;3:cm1.
65. Hirai H, Zhang P, Dayaram T, Hetherington CJ, Mizuno S, Imanishi J, et al. C/EBPβ is required for "emergency" granulopoiesis. Nat Immunol. 2006;7:732–9.
66. Jones SA, Jenkins BJ. Recent insights into targeting the IL-6 cytokine family in inflammatory diseases and cancer. Nat Rev Immunol. 2018;18:773–89.
67. Wellenstein MD, de Visser KE. Cancer-Cell-Intrinsic Mechanisms Shaping the Tumor Immune Landscape. Immunity. 2018;48:399–416.
68. Kiss M, Halasz L, Hadadi E, Berger WK, Tzerpos P, Poliska S, et al. Epigenomic preconditioning of peripheral monocytes determines their transcriptional response to the tumor microenvironment. NCBI Gene Expression Omnibus, Accession number GSE268992, 2025. https://www.ncbi.nlm.nih.gov/geo/query/acc.cgi?acc=GSE268992.

Publisher's Note